ISBN: 978-3-95450-262-2 ISSN: 2673-5350 doi: 10.18429/JACoW-IBIC2025-MOBC02

PERFORMANCE STUDY OF FAST BEAM CURRENT TRANSFORMER CALIBRATION IN THE LHC

J. Marafuz Gaspar*,[1], T. Levens, D. Alves, M. Gasior, K. Lasocha, CERN, Geneva, Switzerland
[1]also at Instituto Superior Técnico, Lisbon, Portugal

Abstract

Fast Beam Current Transformers (FBCTs) are essential devices for measuring bunched beam intensities in the Large Hadron Collider (LHC). A cross-calibration of these devices against DC Beam Current Transformers (DC-BCTs) is used in the LHC ring, but this method relies on assumptions that introduce inaccuracies. FBCTs are also used in the LHC transfer lines, where DC-BCTs are unavailable, making absolute calibration crucial for transmission studies. To allow absolute calibration, the FBCTs are equipped with a pulsed current source to perform a calibration before each fill. However, a systematic underestimation in the calculated scaling factors has been observed when comparing them to the cross-calibration with the DC-BCTs. This work characterizes the calibrator performance, evaluates different algorithms for calculating the scaling factors and reports on issues found linked to processing chain modeling inaccuracies, ghost/satellite bunches, and the FPGA-based digital integration. A revised model of the processing chain improved calibration accuracy by 0.4 %, while an initial test of a batch-by-batch baseline in the digital integration seems to explain the remaining 3 % underestimation.

INTRODUCTION

Accurate measurement of beam intensity is essential for both accelerator operation and, as it is an input used to calculate luminosity, for physics analysis at the Large Hadron Collider (LHC). Beam intensity corresponds to the number of particles in the beam and is measured by dedicated instruments, with Beam Current Transformers (BCTs) being the standard devices used for this purpose.

DC Beam Current Transformers (DC-BCTs) measure the total circulating charge, including bunched and unbunched particles. Since they can be calibrated using accurate DC current sources, they provide a highly stable reference with a long-term accuracy of about ±0.3 % [1]. Fast Beam Current Transformers (FBCTs), in contrast, can resolve the individual bunch charge. They are periodically cross-calibrated against the DC-BCTs in the LHC ring, and this cross-calibration is designed to achieve ±1 % accuracy [2].

Cross-calibration has important limitations. It can only be performed during/after the energy ramp to ensure that all uncaptured beam particles (invisible to the FBCTs) will have been lost, and therefore cannot be systematically repeated before every fill. Moreover, in the LHC transfer lines where no DC-BCTs are available, the FBCTs cannot be cross-calibrated. These constraints reduce the accuracy of bunch intensity monitoring, especially for transmission studies.

* joao.marafuz.gaspar@tecnico.ulisboa.pt

To overcome these challenges, the LHC FBCTs have been equipped with a precise pulsed current source that enables absolute calibration without relying on DC-BCTs [3] with the aim that the calibration can be executed before every fill. The calibration system has so far only been demonstrated as a proof of principle and requires further development before it can be routinely used in LHC operation [4].

This paper addresses this need by characterizing the calibration unit as well as developing and evaluating algorithms for calculating absolute calibration scaling factors from the measured FBCT data. The observed systematic underestimation of the absolute calibration scaling factors relative to cross-calibration is shown to be linked with the processing chain modeling inaccuracies, ghost and satellite bunches, and FPGA-based baseline removal and digital integration.

CROSS-CALIBRATION

During the energy ramp, and in particular in the 1 to 6 TeV energy range, the FBCT and the DC-BCT should ideally measure the same beam intensity, as any unbunched particles are rapidly lost. The correction factor α is determined as the mean ratio of the two signals within the 1 to 6 TeV interval. Applying α to the self-calibration scaling factor C_{CAL} yields the cross-calibration factor $C'_{\mathrm{CAL}} = \alpha C_{\mathrm{CAL}}$, effectively overlapping the two measurements, as shown in Fig. 1. Before the energy ramp, the FBCT signal deviates from the DC-BCT reference due to the presence of uncaptured particles in the beam.

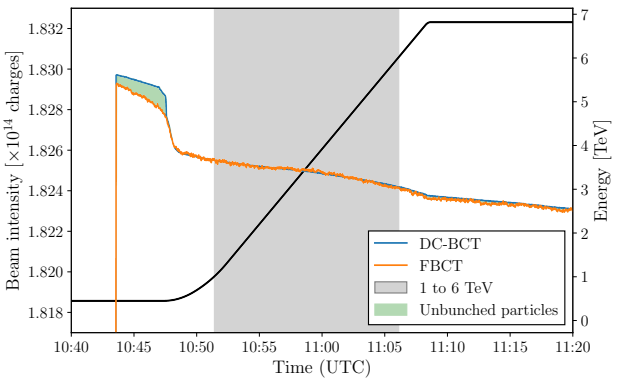

Figure 1: FBCT and DC-BCT beam intensity comparison after cross-calibration for LHC Beam 1 (fill 9523) on 15/04/2025, with the corresponding LHC energy also shown.

ABSOLUTE CALIBRATION

FBCT Processing Chain

Each LHC FBCT consists of a CERN designed Wall Current Transformer (WCT) [4] and a front-end processing chain

ISBN: 978-3-95450-262-2 ISSN: 2673-5350 doi: 10.18429/JACoW-IBIC2025-MOBC02

that conditions the signal before digitization, as shown in Fig. 2. At the output of the WCT signal combiner, a 220 MHz Low-Pass Filter (LPF) stretches the fast bunch signals in time to limit the peak voltage seen by the head-amplifier and to increase the number of digitized samples within the bunch structure. The head-amplifier, located in the tunnel, provides initial amplification and splits the signal into two gain ranges. Between the tunnel and underground technical gallery, the signal is transmitted through 7/8" coaxial cables of length $\ell \approx 24$ m. Finally, there is a distribution amplifier which provides final conditioning of the signal, including a 80 MHz LPF. Digitization is performed by an Analog-to-Digital Converter (ADC) running asynchronously at a sampling frequency of $f_S = 650$ MHz. Real-time digital integration of the sampled signal is performed in an FPGA providing bunch-by-bunch intensity measurements at a rate of 25 Hz.

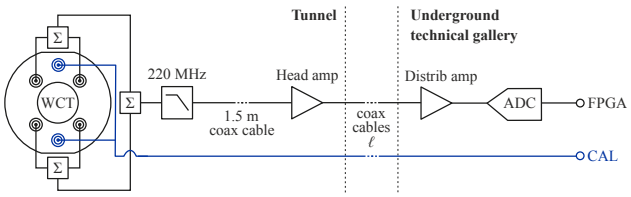

Figure 2: Schematic of the FBCT processing chain.

The system can operate in two distinct modes: beam mode, where bunched beam signals are measured continuously, and calibration mode, where a pulsed current source is injected for absolute calibration.

Beam Mode In beam mode, the circulating bunches traverse the WCT, inducing a voltage that is processed by the FBCT chain. As shown in Fig. 3, the LPF stretches the beam waveform in time without altering its DC component, so the integral of the signal is conserved. This increases the effective sampling resolution from fewer than two points per bunch, for a typical length of $4\sigma = 1.1$ ns, to about 16 ADC samples.

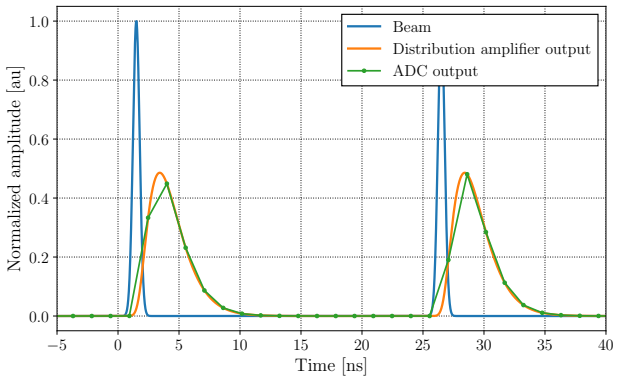

Figure 3: Simulated time response of the FBCT processing chain in beam mode, showing the increased sampling resolution after filtering.

Calibration Mode In calibration mode, a 250 µs pulse from the reference source [3] is injected into the calibration winding of the FBCT, as illustrated in Fig. 4. While calibration using nanosecond-scale pulses would better resemble the bunch structure, achieving ppm-level stability from a current source at such timescale is not feasible. The primary objective, however, is amplitude calibration rather than temporal resolution: the time axis relevant for integral evaluation is already well defined by the precise clocking of the ADC. A calibration pulse with ppm-level amplitude accuracy is achieved using a long pulse generated by a circuit with a finely regulated feedback loop [3].

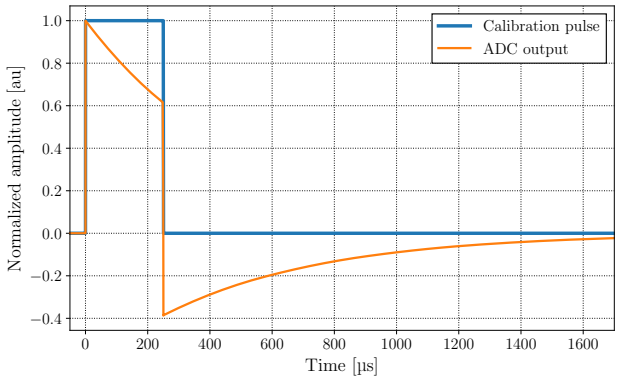

Figure 4: Simulated time response of the FBCT processing chain in calibration mode, showing the droop of the output signal.

The purpose of the calibration is to determine the scaling factor that converts raw ADC samples into beam intensity. This is obtained by comparing the known calibration current $i_{\mathrm{CAL}}(0)$ with the ADC output at the origin $y_{\mathrm{ADC}}(0)$ as

$$C_{\mathrm{CAL}} = \frac{i_{\mathrm{CAL}}(0)}{y_{\mathrm{ADC}}(0)} \times \frac{T_S}{e}\ [\mathrm{charges/ADC\ bins}], \qquad (1)$$

where $T_S = 1/f_S$ is the sampling period and e the elementary charge.

As shown in Fig. 4, the response exhibits a droop. This is due to the lack of DC response from the FBCT, which can be modeled as a first-order high-pass system with time constant $\tau_{\mathrm{FBCT}} \approx 360$ µs. The system's transfer function is thus given by

$$H(s) = K\frac{s}{s + \frac{1}{\tau_{\mathrm{FBCT}}}}, \qquad (2)$$

leading to the steady-state output response

$$y_{\mathrm{ADC}}(t) = Ke^{-\frac{t}{\tau_{\mathrm{FBCT}}}}, \quad t \in (0, T_{\mathrm{pulse}}), \qquad (3)$$

and equivalently described by the differential equation

$$i'_{\mathrm{FBCT}}(t) + \frac{1}{\tau_{\mathrm{FBCT}}} i_{\mathrm{FBCT}}(t) = i'_{\mathrm{CAL}}(t). \qquad (4)$$

An additional challenge arises from impedance mismatches. The WCT is designed with a 10 Ω input calibration resistance for the reasons detailed in [4], whereas the

ISBN: 978-3-95450-262-2 ISSN: 2673-5350 doi: 10.18429/JACoW-IBIC2025-MOBC02

transmission cables have the standard 50 Ω characteristic impedance. This mismatch leads to signal reflections that become more pronounced with increasing cable length ℓ, and notoriously distort the signal in the vicinity of the initial transient, as illustrated in Fig. 5, where $\ell \approx 24$ m.

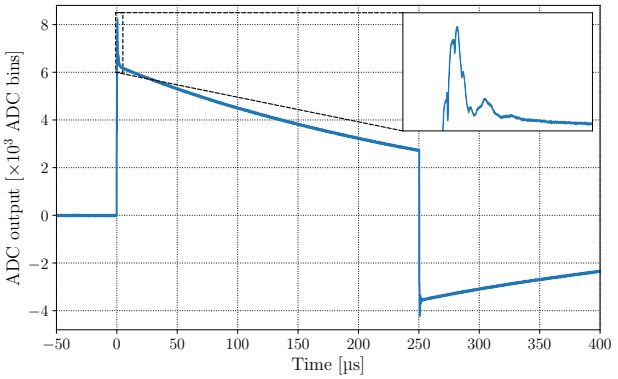

Figure 5: Time response of the FBCT processing chain to a standard calibration pulse on 01/05/2025, showing the impedance mismatch effect.

Equation (1) requires an accurate value of $y_{\mathrm{ADC}}(0)$, but, because of the signal reflections, the direct use of the measured signal for the calibration is not reliable. Additional logic is therefore essential to compensate for these distortions, motivating the development of dedicated algorithms for absolute calibration.

Estimation Algorithms for Calibration

With the knowledge of $i_{\mathrm{CAL}}(0)$, the scaling factor in Eq. (1) can be determined provided an accurate estimate of $y_{\mathrm{ADC}}(0)$ is available. However, as shown in the previous section, distortions near the origin hinder a direct measurement of this quantity. To overcome this limitation, two estimation algorithms were developed that infer $\hat{y}_{\mathrm{ADC}}[0]$ from portions of the signal less affected by reflections.

Algorithm I estimates the signal at the origin by fitting and extrapolating a model function, as shown in Fig. 6. The fit function f is derived from Eq. (3), where the parameters to be estimated are the set θ, in this case $\theta = \{K, \tau_{\mathrm{FBCT}}\}$. While this technique provides a straightforward estimation, it relies on a single extrapolated point at an arbitrarily chosen origin, which may introduce variability across calibrations. Sensitivity tests conducted by shifting the origin within a ± 1 µs range showed only a minor impact on accuracy, within ± 0.1 %, but this dependency motivated the development of an alternative solution.

Algorithm II takes a different approach by using the system model, given by Eq. (4), to numerically reconstruct the shape of the calibration current i_{CAL}, as shown in Fig. 7. This technique requires an estimate of the time constant $\hat{\tau}_{\mathrm{FBCT}}$ obtained from the previous algorithm. Unlike Algorithm I, this technique averages over multiple samples of the reconstructed signal within a time window, rather than relying on a single extrapolated point. This makes the estimation

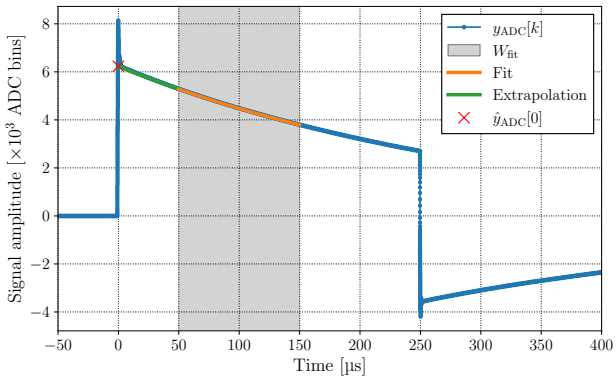

Figure 6: Illustration of Algorithm I using ADC output data from 01/05/2025.

more robust to signal distortions and noise, improving the calibration quality.

Estimation Algorithm II

Require: Differential equation $y'_{\mathrm{CAL}}(t) = f(t, y_{\mathrm{ADC}}[k])$ given by Eq. (4), discrete-time raw data signal $y_{\mathrm{ADC}}[k]$, and gated averaging window W_{gate}.

Algorithm:

1: Retrieve the estimated parameters $\hat{\theta}$ from Algorithm I.
2: Numerically solve the system's differential equation using Euler discretization with step size h and initial condition $\hat{y}_{\mathrm{CAL}}[0] = 0$:
3: **loop**

$$\hat{y}_{\mathrm{CAL}}[k+1] = \hat{y}_{\mathrm{CAL}}[k] + hf(k, y_{\mathrm{ADC}}[k:k+1]) \quad (5)$$

4: $k \leftarrow k + 1$
5: **end loop**
6: Compute the average of $\hat{y}_{\mathrm{CAL}}[k]$ within the window:

$$\hat{y}_{\mathrm{ADC}}[0] = \frac{1}{\|W_{\mathrm{gate}}\|} \sum_{k \in W_{\mathrm{gate}}} \hat{y}_{\mathrm{CAL}}[k] \quad (6)$$

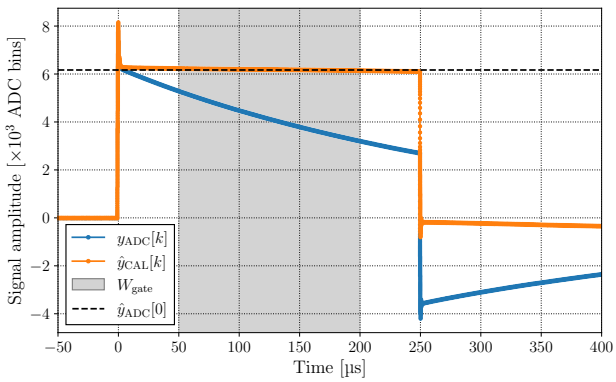

Figure 7: Illustration of Algorithm II using ADC output data from 01/05/2025.

ISBN: 978-3-95450-262-2 ISSN: 2673-5350 doi: 10.18429/JACoW-IBIC2025-MOBC02

ACHIEVED RESULTS

Absolute vs. Cross-calibration

In principle, scaling factors from absolute calibration should match those from cross-calibration, yielding a constant ratio of 100 % over time; however, this is not observed in practice. As shown in Fig. 8, absolute calibration exhibits a systematic underestimation of 3–4 %. Unexpectedly, Algorithm II, which exploits more data, appears less stable than Algorithm I. The cause of this behavior is still being investigated. The following three sections discuss potential causes for this underestimation.

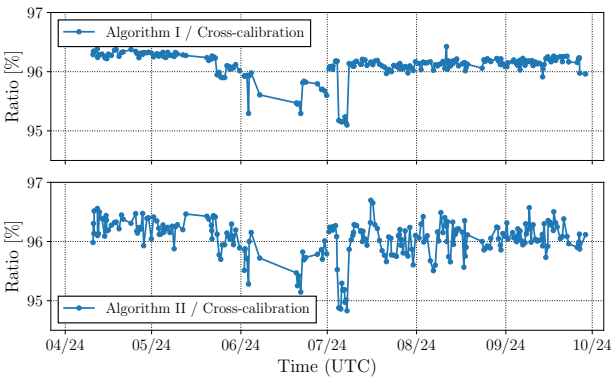

Figure 8: Evolution of the ratio between absolute and cross-calibration scaling factors for LHC Beam 1 over 2024, shown for both estimation algorithms. The presented results were obtained with $W_{\text{fit}} = [50, 150]$ µs and $W_{\text{gate}} = [50, 200]$ µs.

Inaccurate Fit Function

The FBCT processing chain is modeled as a first-order high-pass filter, leading to a characteristic described by Eqs. (3) and (4). This simplified approximation may lead to an error in estimating $\hat{y}_{\text{ADC}}[0]$ when applied in Algorithms I and II. For instance, the head and distribution amplifiers present in the FBCT processing chain are not DC coupled. This design avoids an accumulation of temperature-dependent DC offsets, which could otherwise degrade the system performance. However, this choice introduces additional low-frequency cutoffs, and alters the effective system response. When tested individually in the laboratory with a calibration pulse, the head and distribution amplifiers were found to exhibit time constants about 60 and 8 times higher than the FBCT, respectively.

To account for this, the amplifiers were modeled as additional first-order high-pass filters, yielding a cascade of three systems,

$$H(s) = H_{\text{FBCT}}(s)H_{\text{HAmp}}(s)H_{\text{DAmp}}(s) = K\frac{s}{s+a}\frac{s}{s+b}\frac{s}{s+c}, \quad (7)$$

where $a = 1/\tau_{\text{FBCT}}$, $b = 1/\tau_{\text{HAmp}}$ and $c = 1/\tau_{\text{DAmp}}$. The corresponding time-domain response was derived as

$$y_{\text{ADC}}(t) = K\frac{a^2(b-c)e^{-at} + b^2(c-a)e^{-bt} + c^2(a-b)e^{-ct}}{(a-b)(a-c)(b-c)}, \quad (8)$$

valid for $t \in (0, T_{\text{pulse}})$. The resulting time-domain response was applied to the data, improving calibration accuracy by about 0.4 %, as shown in Fig. 9. While this reduces the bias, it does not fully explain the observed underestimation.

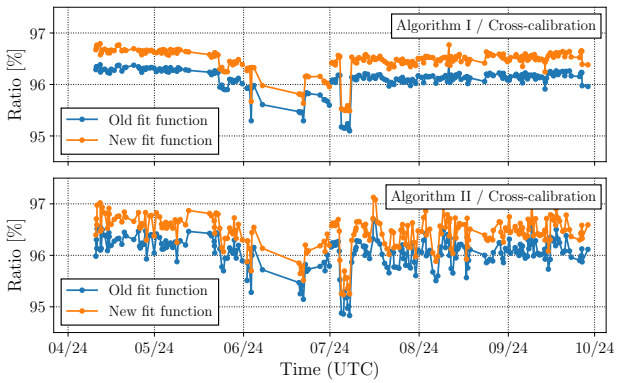

Figure 9: Evolution of the ratio between absolute and cross-calibration scaling factors for LHC Beam 1 over 2024, shown for both estimation algorithms and for both old and new fit functions, given by Eqs. (3) and (8), respectively.

Satellites and Ghosts

Satellites, which are parasitically populated RF bins in the vicinity of nominal bunches, and ghosts, which are charges located in nominally unpopulated bunch slots, arise from imperfect capture or injection processes [5]. Their charge is measured by the DC-BCTs but, due to the signal processing used, they are not detected by the FBCTs. This artificially raises the cross-calibration scaling factors and lowers the ratios of absolute to cross-calibration.

The contribution due to the presence of these residual bunches was estimated from Longitudinal Density Monitor (LDM) data [6]. Figure 10 shows the resulting satellite fractions together with the corresponding cross-calibration scaling factors. There is a noticeable correlation: higher satellite fractions correspond to higher cross-calibration scaling factors and therefore to lower ratios, confirming satellites' influence. Nevertheless, since these fractions remain at the sub-percent level, they still do not fully explain the systematic underestimation but contribute to its variability. Ghosts contribute less than 0.1 % with no observed relationship to the cross-calibration scaling factors, so their contribution is negligible in this analysis.

Digital Integration

The real-time processing performed by the FPGA may also underestimate the total charge. This can be due to the baseline correction logic, performed before the numerical integration of the bunch charge. The current method computes a bunch-by-bunch baseline for each set of 16 ADC samples by averaging its first and last points.

Alternative strategies for baseline estimation were tested offline. In the so-called *abort gap baseline* approach, the baseline is calculated as the average of the samples taken between bunch slots 3445–3564, corresponding to the 3 µs

ISBN: 978-3-95450-262-2 ISSN: 2673-5350 doi: 10.18429/JACoW-IBIC2025-MOBC02

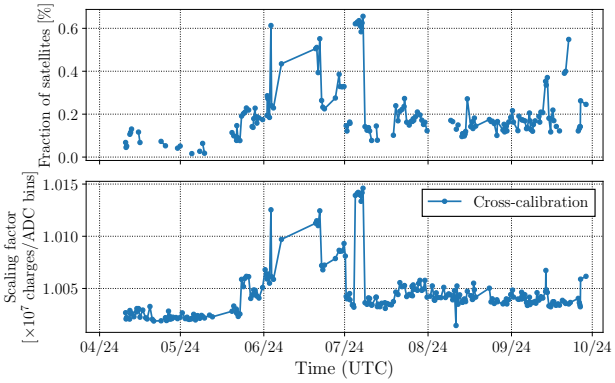

Figure 10: Evolution of the satellite fraction from LDM measurements and the corresponding cross-calibration scaling factor for LHC Beam 1 over 2024. A strong linear relationship is observed between the two quantities (R^2 = 0.825).

region intentionally left unpopulated at the end of the *turn*. In the so-called *batch-by-batch baseline* approach, the average of the samples in the bunch slots, immediately before and after each batch, is used. When applied to the LHC fill 10219, both alternatives yielded higher integrated intensities than the bunch-by-bunch baseline method, as shown in Fig. 11.

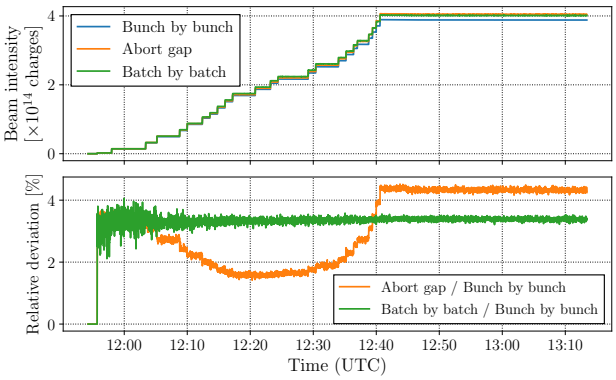

Figure 11: Comparison of baseline methods for beam-intensity calculation using ADC output data for LHC Beam 1 (fill 10219) on 12/10/2024.

The relative deviation between the abort gap baseline and the bunch-by-bunch baseline methods exhibits a non-monotonic behavior, with the values spanning 2.5–4.5 %, which can be attributed to the droop caused by the AC response of the FBCT. During injection, as new particle batches are added to the accelerator, the abort gap baseline decreases due to increased beam-induced droop until the machine reaches approximately half capacity. At this point, the relative deviation reaches its minimum, likely because the balance between the injected beam current and the system's droop response stabilizes. After the last injection, the baseline stabilizes, resulting in a constant relative deviation.

By contrast, the relative deviation between the batch-by-batch baseline and the bunch-by-bunch baseline methods demonstrated a constant value around 3 %, indicating that the batch-by-batch baseline method showed a constant ~3 % increase, directly comparable to the systematic underestimation observed in absolute calibration.

CONCLUSIONS

This study demonstrated that absolute calibration of FBCTs is feasible but consistently yields scaling factors that are 3–4 % lower than those obtained from cross-calibration with DC-BCTs. Three main contributors to this systematic underestimation were identified: (i) inaccuracies in the simplified processing chain model, (ii) the effect of satellites and ghosts that artificially increase the DC-BCT reference, and (iii) issues with the FPGA baseline correction logic. An improved chain model incorporating additional low-frequency filtering reduced the discrepancy by about 0.4 %, while the analysis of parasitic bunches revealed their role in introducing variability despite their sub-percent fractions. Finally, reproducing offline the baseline compensation method implemented in the FPGA was shown to be the main contributor to the observed relative deviations of approximately 3 % in terms of the absolute calibration factors with respect to the cross-calibration method. As a natural consequence of this study, the most promising baseline removal method (batch-by-batch) will be implemented in the online system and benchmarked during the short LHC run in 2026.

ACKNOWLEDGMENTS

The authors would like to thank their colleagues from the SY-BI-IQ section at CERN for their support, with special thanks to Ole Marqversen for his help and insightful discussions. We are also deeply grateful to the late Stefano Mazzoni, whose contributions and guidance were invaluable to the section.

REFERENCES

[1] M. Palm *et al.*, *LHC Beam Current Measurements: Performance and Issues in Run 2, Prospects for Run 3*, presented at the LHC Lumi Days 2019, CERN, Geneva, Switzerland, 2019, https://indico.cern.ch/event/813285/contributions/3406074

[2] C. Fischer, and R. Schmidt, *On the Measurements of the Beam Current, Lifetime and Decay Rate in the LHC Rings*, CERN, Geneva, Switzerland, Rep. LHC-BCT-ES-0001, 2005. https://edms.cern.ch/document/359172/1.0

[3] M. Krupa and M. Gasior, "A Precise Pulsed Current Source for Absolute Calibration of Current Measurement Systems With No DC Response", in *Proc. IBIC'16*, Barcelona, Spain, Sep. 2016, pp. 165–168. doi:10.18429/JACoW-IBIC2016-MOPG49

[4] M. Krupa, "A Wall Current Transformer for Beam Intensity Measurements in the Large Hadron Collider", PhD thesis, CERN, Geneva, Switzerland, 2022. https://cds.cern.ch/record/2842364

[5] A. Alici *et al.*, *Study of the LHC ghost charge and satellite bunches for luminosity calibration*, CERN, Geneva, Switzerland, Rep. CERN-ATS-2012-029 (PERF), 2012. https://cds.cern.ch/record/1427728

[6] A. Jury *et al.*, "Performance Analysis of the LHC BSRL and Possible Improvements", presented at IBIC'25, Liverpool, UK, Sep. 2025, paper MODC02, this conference.